Microstructures and Mechanical Properties of Pure V and Mo Processed by High-Pressure Torsion

Seungwon Lee, Kaveh Edalati and Zenji Horita

Department of Materials Science and Engineering, Faculty of Engineering, Kyushu University, Fukuoka 819-0395, Japan

Two body centered cubic (bcc) metals, V and Mo, were processed by high pressure torsion (HPT) at ambient temperature. Hardness variation as well as microstructural evolution was examined with strain under a pressure of 2 to 6 GPa. It was shown that the hardness increases with straining and saturates to a constant level with the grain size of 330–400 nm in V irrespective of the applied pressures. Although the hardness variation with strain is the same for Mo with the grain size of ∼350 nm at the saturation level when the applied pressure is 6 GPa, the hardness level lowers below the saturation level and the grain size becomes coarser as the pressure is lowered. Tensile tests show that the strength significantly increases with some ductility for V after processing under any pressure and for Mo under lower pressures, but brittle fracture occurs in the Mo specimen processed at 6 GPa. The slower evolution of microstructure as well as the lower hardness levels observed in Mo is due to the applied pressure which is lower than the yield stress and thus due to the insufficient generation of dislocations for grain refinement.   [doi:10.2320/matertrans.M2009375]

1. Introduction

Materials with small grain sizes have several advantages over their coarse-grained counterparts because they have higher strength and better ductility. The significance of grain refinement by severe plastic deformation (SPD) was recognized almost 2 decades ago.[1] Several methods were developed for the SPD process, which include equal-channel angular pressing (ECAP), high-pressure torsion (HPT), accumulative roll bonding (ARB), multi directional forging (MDF), cyclic extrusion and compression (CEC) and repetitive corrugation and strengthening (RCS).[2] In particular, the HPT process produces grain sizes finer than the other processes[3] and it is possible to apply to hard materials and powder consolidation without heating process.[4,5] The principle of the HPT processing is that the sample, in the form of a disk or a ring, is placed between two anvils which are rotated with respect to each other under application of compressive pressure, P, of several GPa to create a torsional strain in the sample.[6] Using the HPT process, researches were conducted on many face-centered cubic (fcc) metals and alloys[7,8] including hexagonal-closed packed (hcp) metals and alloys.[9] However, except for Fe and its alloys, there are few researches on body-centered cubic (bcc) metals and alloys and thus, it should be worth investigating grain refinement behavior of bcc structure materials using the HPT process.

There are twelve kinds of bcc metals according to periodic table. Among them, it is possible to apply practically the HPT process to 7 metals such as V[23], Cr[24], Fe[26], Nb[41], Mo[42], Ta[73] and W[74] in 5, 6 groups and 4, 5, 6 periods on the periodic table. For the other 5 bcc metals such as Na[11], K[19], Rb[37], Cs[55] and Ba[56], it is not easy to apply the HPT process because they have low melting points and are susceptible to oxidation at room temperature. Although many reports are available for Fe,[10–13] very limited applications have been reported on the bcc metals using the HPT process.[14–19]

In this research, two bcc metals, V and Mo, are selected because not only there are few studies using the HPT process but also there is a marked difference in the strength between V and Mo where V is softer and lower melting point (2136 K) but Mo is harder and higher melting point (2883 K).

2. Experimental Materials and Procedures

The materials used in this research were high purity V (99.9%) and Mo (99.9%). They were purchased in a form of $10 \times 10 \times 1$ mm³ chips and these chips were rolled down to a thickness of 0.85 mm. Disks of 0.85 mm thickness and 10 mm diameter were then cut by a wire-cutting electric discharge machine (EDM). The disks were processed by HPT under a selected pressure of 2, 4 and 6 GPa with 1/4, 1, 2, 5 or 10 revolution at a rotation speed of 1 rpm at room temperature. The alignment around the rotation axis of the upper and lower axes was adjusted to well within ±0.01 mm. Slippage between the disk and the anvils was measured after 1/4 revolutions as described earlier.[7]

The disks were mechanically polished to a mirror-like surface and the Vickers microhardness was measured along the 12 radial directions at every 0.5 mm from the disk center to the edge. The average was calculated from the twelve separate measurements at the same distances from the center. The disk processed for 5 revolutions at each pressure was cut to two halves and polished to a mirror-like surface and the hardness measurements were also conducted across the thickness on the cross sectional plane at every 0.08 mm from one surface to the other. Each hardness measurement was conducted by using a load of 200 g for a duration time of 15 s.

After processing by HPT, the disks were mechanically polished to a thickness of ∼0.50 mm and tensile specimens were cut from the polished disks using the EDM at the 2 mm off-center position as illustrated in Fig. 1 with the dimensions of 1.5 mm gauge lengths and 0.7 mm widths. The tensile
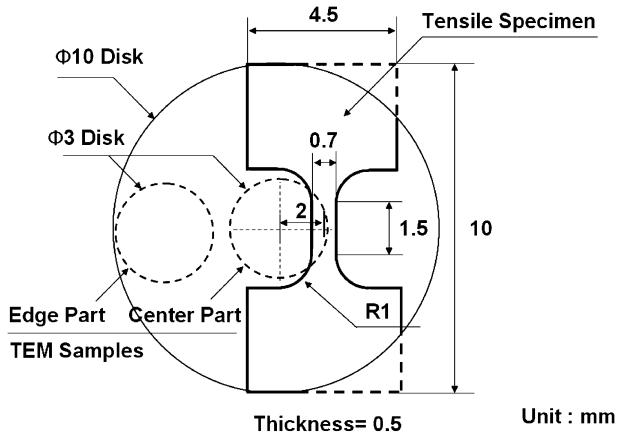
Fig. 1   Dimensions of disk sample including positions for TEM disks and tensile specimen.
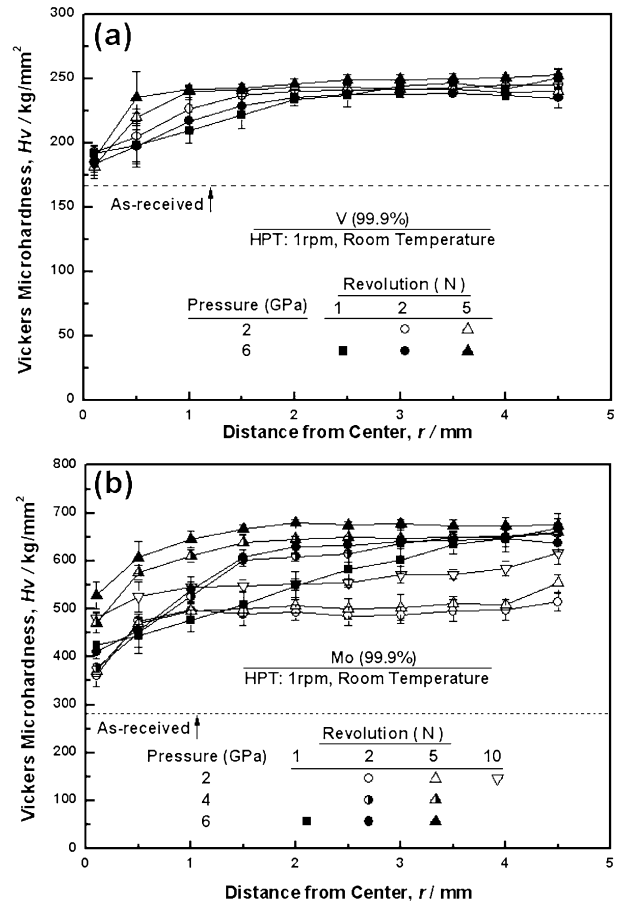

Fig. 2   Vickers microhardness plotted against distance from center for (a) V and (b) Mo after HPT processing at 2, 4 and 6 GPa for various revolutions.

specimens were pulled to failure at a room temperature using a testing machine operating at a constant rate of cross-head displacement with the initial strain rate of $3.0 \times 10^{-3}\,\text{s}^{-1}$. The fracture surface was observed by a Keyence VE7800 scanning electron microscope (SEM) operating at 20 kV.

Disks with 3 mm diameter were punched out from the center and edge parts of HPT-processed disks as illustrated in Fig. 1. They were ground to a thickness of 0.15 mm and then thinned using a twin-jet electro-polishing facility in a solution of 10 vol% H_2SO_4 and 90 vol% CH_3OH at 253 K with an application of 13.5 V for Mo, and a solution of 90 vol% CH_3COOH and 10 vol% $HClO_4$ at room temperature with an application of 29 V for V. The microstructures were observed using a Hitachi H-8100 transmission electron microscope (TEM) operating at 200 kV. Selected area electron diffraction (SAED) patterns were taken from regions having diameters of 6.3 µm.

3.   Results and Discussions

3.1   Hardness variations

Vickers microhardness is plotted against the distance from the disk center after HPT processing in Fig. 2(a) for V and in Fig. 2(b) for Mo. For both metals, the microhardness increases with increasing distance from the center and saturates to a constant level. The hardness increase is faster as the applied pressure is higher and the number of the revolution is larger as reported in other metals.[6,7,10] However, there is a significant difference between the results of V and Mo. First, the hardness level at the saturation is much higher in Mo than in V and second, the hardness level at the saturation appears to be dependent on the applied pressure in Mo while it is almost the same in V irrespective of the pressure. These trends are more clearly demonstrated when the hardness data are plotted against the equivalent strain in Fig. 3. Here, the following equation is used for the calculation of the equivalent strain.[7]

$$\varepsilon = (1 - s) \int_0^N \frac{2\pi r}{\sqrt{3}t(N)} \, dN \qquad (1)$$

where r is the distance from the disk center, N is the number of revolutions, s is the fraction of slippage and $t(N)$ is the disk

thickness after HPT processing. The value of s was measured at each pressure for both metals using a procedure as described in an earlier report and was found to be in the rage of 0.2 to 0.25. The form of $t(N)$ was determined as a function of N by measuring the thicknesses after several different revolutions as described earlier.[10]

It is now apparent that the hardness increases with increasing equivalent strain at an initial stage of straining and levels off. Whereas a single level of saturation is achieved in V, the saturation level appears to be different in Mo with the higher level of hardness at the higher applied pressure. Close examination reveals that the levels obtained at the applied pressures of 2 GPa and 4 GPa tend to increase with straining although the increase is very gradual. This suggests that, when the applied pressure is low, the microstructure gradually evolves with straining and reaches a steady state where a balance between hardening and softening is established as described in an earlier report.[20] It should be noted that the evolution at the higher pressure of 6 GPa is similar to the one obtained in Cu, Fe and other metals and alloys.[7,10] It is considered that the slow evolution of hardness at the lower pressures can be due to insufficiency of the pressure compared with the yield strength of Mo. As will be shown later by tensile testing, the yield strength of V is $\sim$300 MPa, whereas that of Mo is $\sim$700 MPa and thus the difference is more than twice.
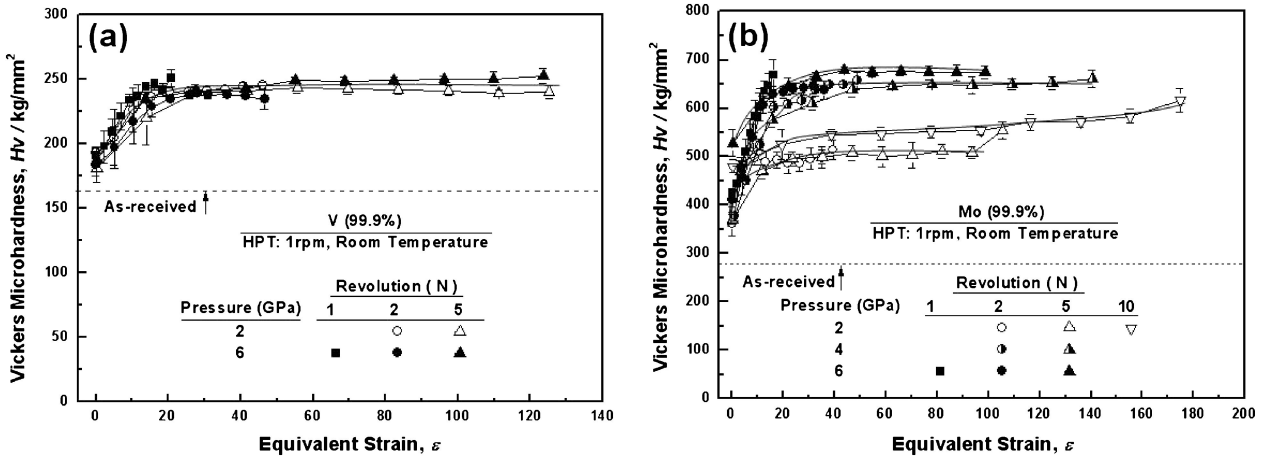
Fig. 3 Vickers microhardness plotted against equivalent strain for (a) V and (b) Mo after HPT processing at 2, 4 and 6 GPa for various revolutions.
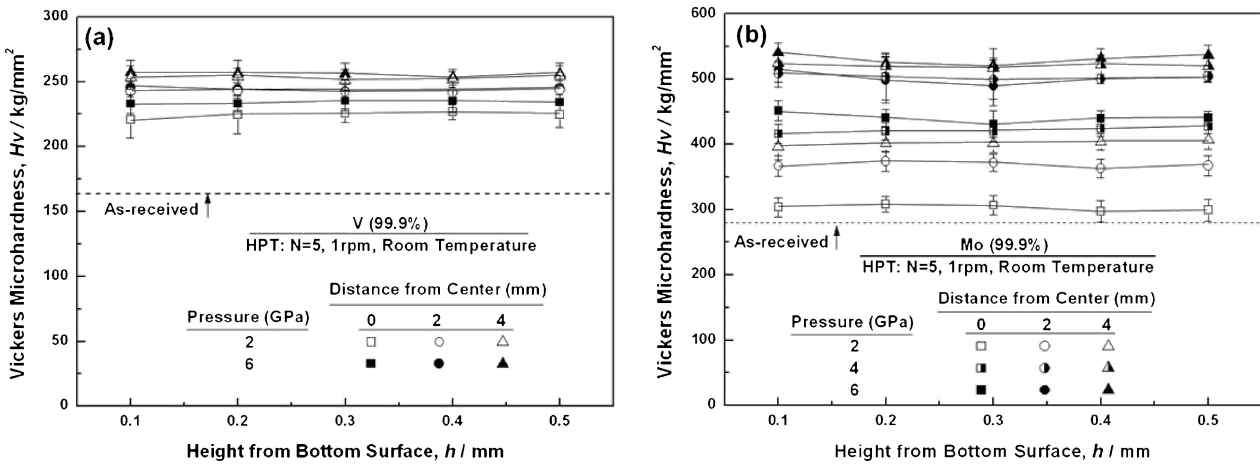

Fig. 4 Vickers microhardness plotted against height from bottom on cross sectional plane for (a) V and (b) Mo.
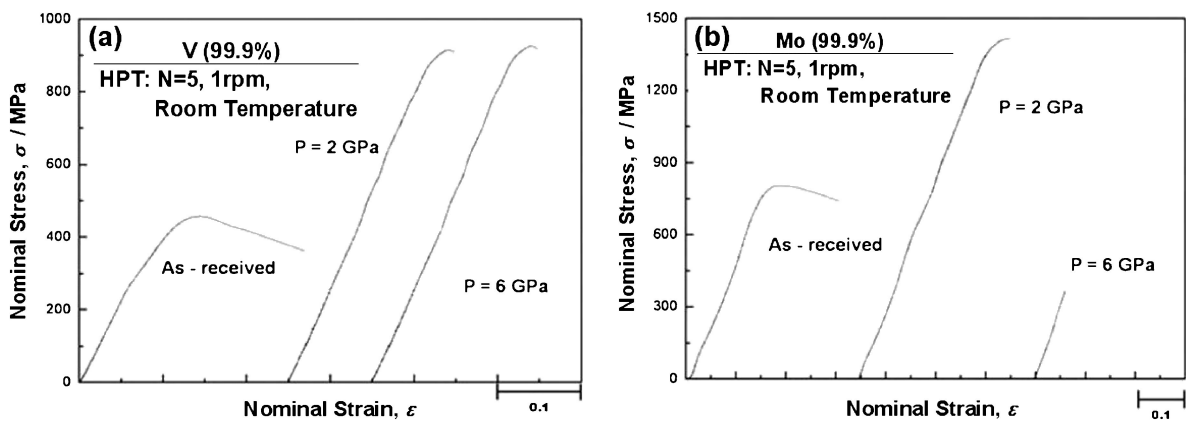

Fig. 5 Nominal stress versus nominal strain curves for (a) V and (b) Mo at pressures of 2 and 6 GPa.

The hardness measurement was also conducted across the thickness at different distances from the disk center to check homogeneity in terms of the hardness. Figure 4 plots hardness values as a function of the height from one side of the disk surface to the other on the cross sectional plane which was cut along the diameter of each disk. Although the hardness level is different for the applied pressure and this difference is much larger in Mo than in V in consistent with the trend shown in Fig. 3, no appreciable variation in the hardness is observed across the thickness in V and Mo. The results suggest that the disk were deformed homogeneously throughout the thickness at any location from the center.
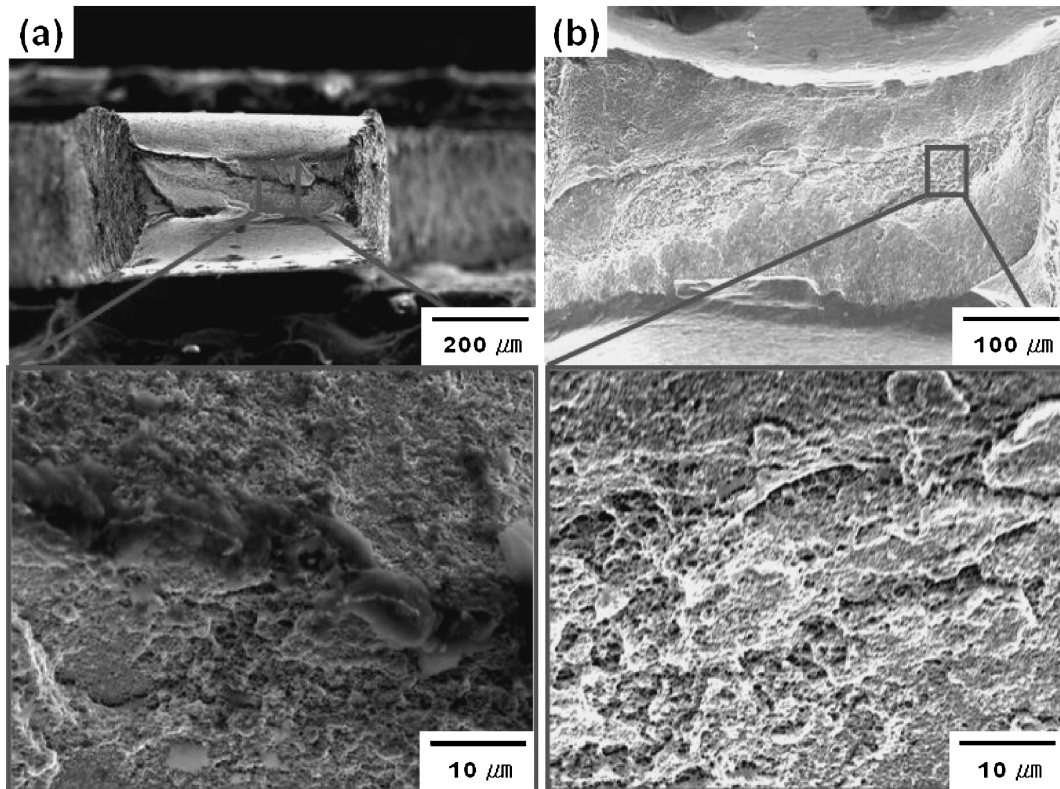
Fig. 6 SEM Fractographs for V: (a) HPT at P = 2 GPa and (b) HPT at P = 6 GPa tensile specimens. Magnified views of selected square areas are shown below overall views.
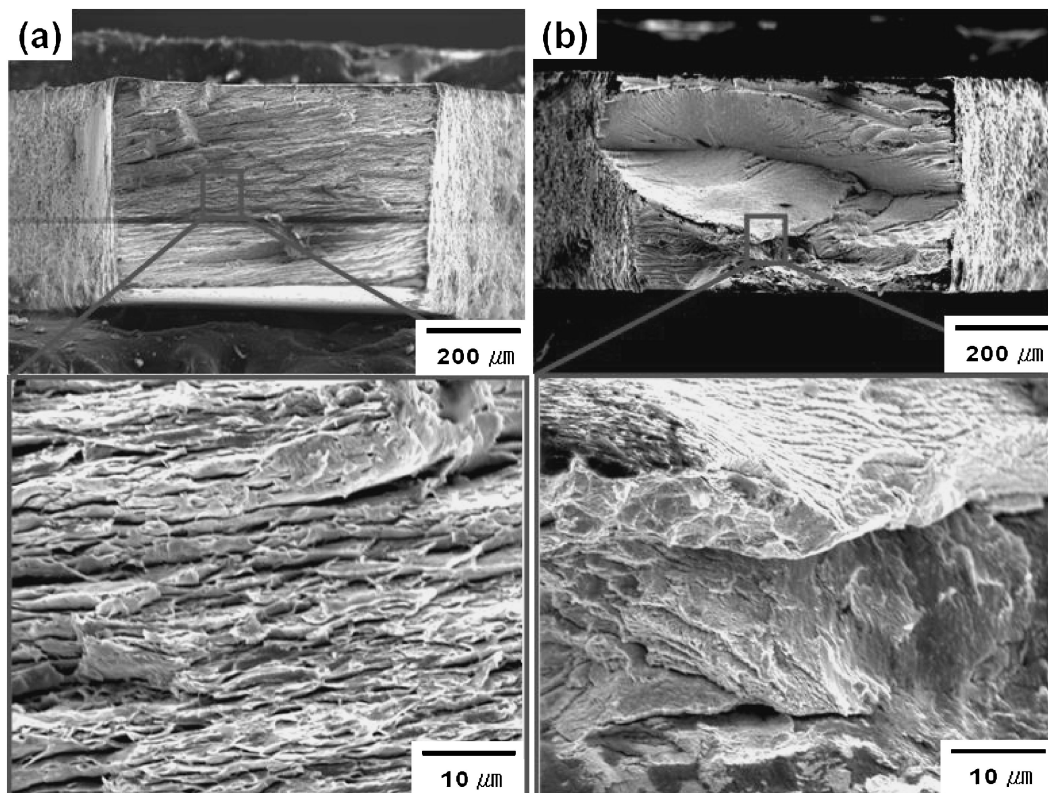

Fig. 7 SEM Fractographs for Mo: (a) HPT at P = 2 GPa and (b) HPT at P = 6 GPa tensile specimens. Magnified views of selected square areas are shown below overall views.
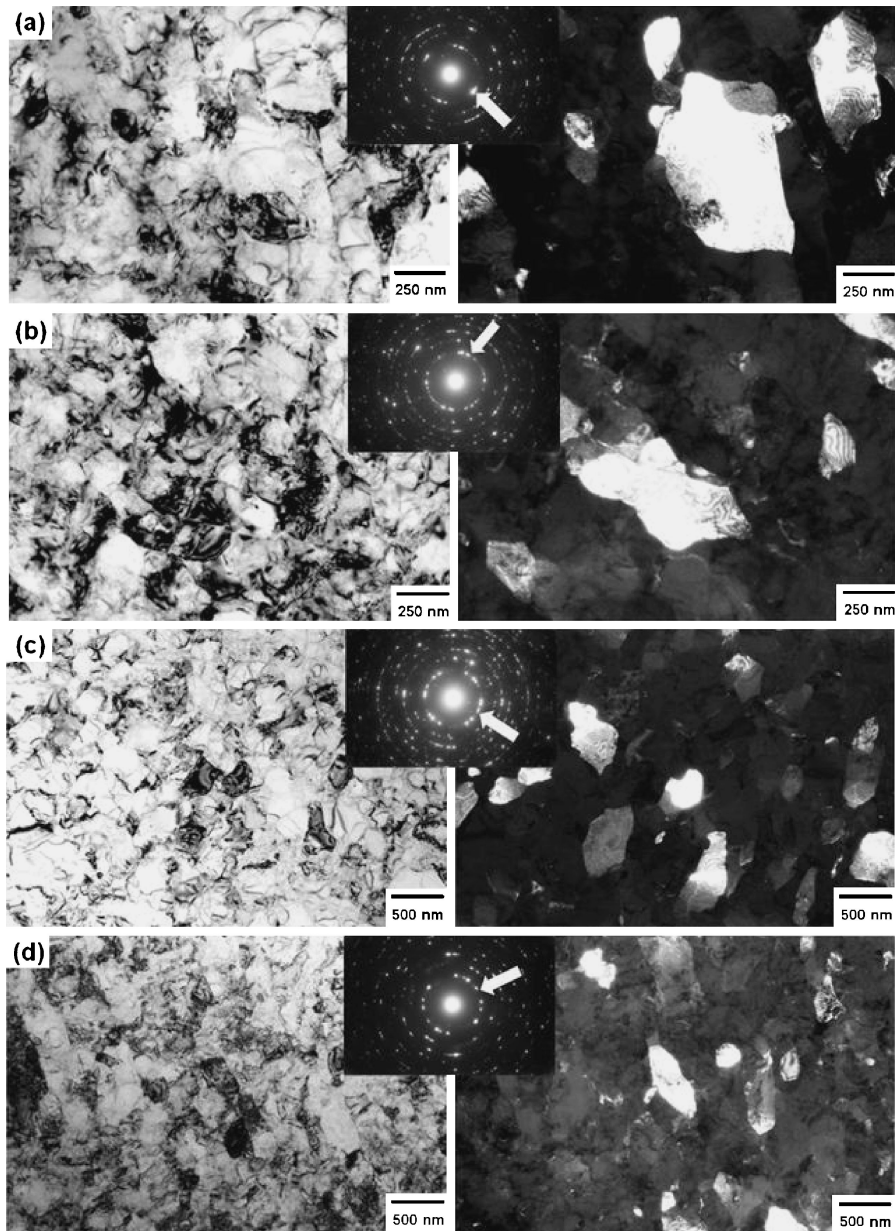
Fig. 8   TEM micrographs and SAED patterns of V: after 5 revolutions at P = 2 GPa near (a) center part and (b) edge part, and at
P = 6 GPa near (c) center part and (d) edge part.

3.2   XRD analysis

Inspection of the XRD profiles confirmed that there are no extra peaks arising from different phases including products formed during HPT operation. It is thus concluded that neither phase transformation nor hydrides formation occurs, unlike metals such as Ti, Zr and Hf reported earlier.[21–23] It is also concluded that the increase in the hardness level observed in Mo is not due to the phase transformation and hydride formation.

3.3   Tensile tests

Strain-stress curves are displayed in Fig. 5(a) and (b) for V and Mo, respectively, from tensile testing conducted at room temperature with an initial strain rate of $3.0 \times 10^{-3} \, \text{s}^{-1}$. The tensile strength is significantly increased by the HPT processing for both V and Mo when compared with the as-received conditions with an elongation to failure retained to

some extent except for the Mo processed under 6 GPa where the tensile specimen failed during loading. It should be noted that V exhibits almost the same tensile strength for both pressures of 2 and 6 GPa and this is consistent with Fig. 2(a) and 3(a) where the hardness levels are the same once they reach the saturation.

4.   Fractography

The fracture surfaces after tensile testing of individual specimens are shown in Fig. 6 and Fig. 7 for V and Mo, respectively, where (a) and (b) correspond to the specimens processed at 2 and 6 GPa. Higher magnification views are shown below the overall views of the fracture surfaces where the selected square regions correspond to the magnified images. Fractograpgy in Fig. 6 shows that there appears to be little difference in the surface morphology
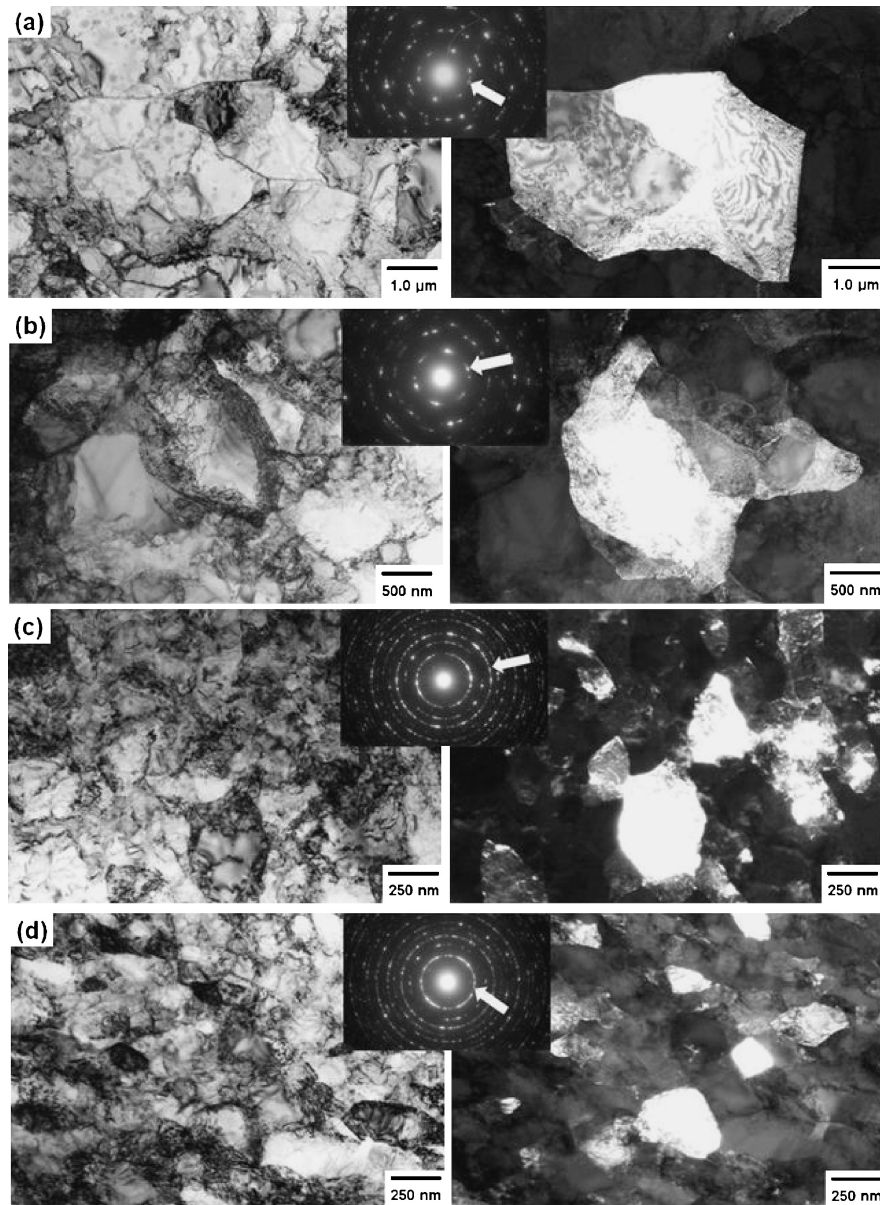
Fig. 9 TEM micrographs and SAED patterns of Mo: after 5 revolutions at P = 2 GPa near (a) center part and (b) edge part, and at P = 6 GPa near (c) center part and (d) edge part.

between the samples processed at 2 and 6 GPa: both sample contain some regions having fine dimple structures on the fracture surfaces and these features are consistent with the stress-strain curves exhibiting some extent of ductility as shown in Fig. 5(a). It is considered that the fine structures after fracture appear to reflect ultrafine-grained structures produced by HPT processing. The difference in the fractography is prominent between the fracture surfaces of the specimens processed at 2 and 6 GPa as shown in Fig. 7(a) and (b). Fine dimple patters are visible for the specimen processed at 2 GPa but the smoother surface exhibits cleavage for the sample at 6 GPa. The latter surface appears because the specimen becomes hardened by intense straining and thus cracks form and propagate through the specimen. These features are then consistent with the fracture modes with some ductility in the former and brittleness in the latter as shown in Fig. 5(b).

5. Transmission Electron Microscopy

Figures 8 and 9 show TEM micrographs including SAED patterns of V and Mo processed for 5 revolutions under 2 and 6 GPa, respectively: in each figure, bright-field images on the left and dark-field images on the right. The dark field images were taken with the diffracted beams indicated by arrows in the SAED patterns. The microstructures obtained under 2 GPa are shown in (a) and (b) and those under 6 GPa are in (c) and (d) for each of Fig. 8 and Fig. 9. As illustrated in Fig. 1, the microstructures were taken from the center parts and edge parts of disks and they are shown in (a) and (c) for the center parts and in (b) and (d) for the edge parts for each of Fig. 8 and Fig. 9. The grain size distributions at the center and edge parts are shown in Fig. 10 and Fig. 11 for V and Mo, respectively, where (a) is for 2 GPa and (b) for 6 GPa. The average grain sizes are given in Table 1. The
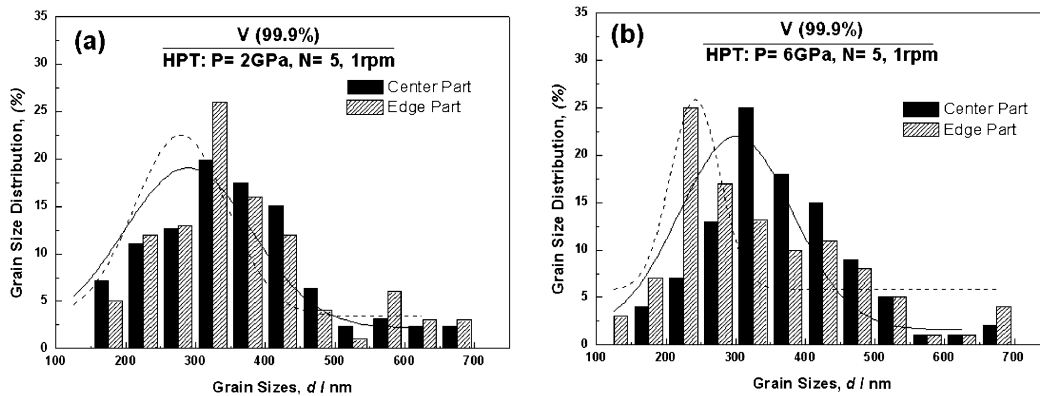
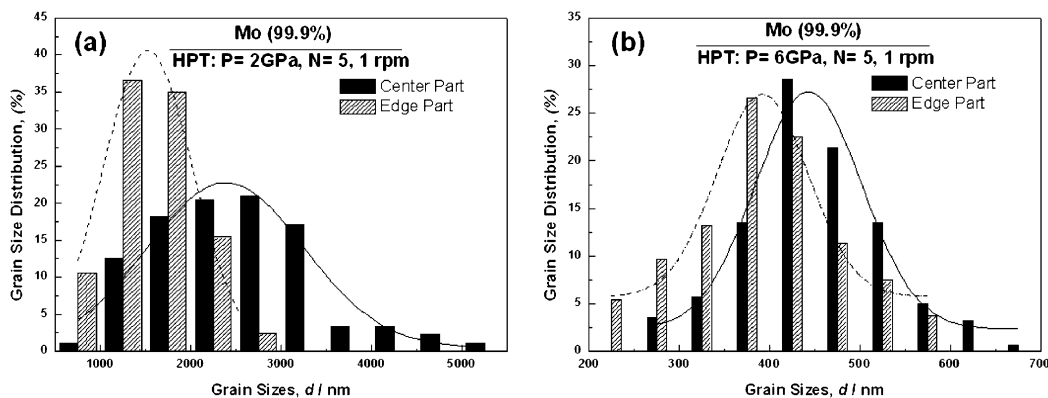Fig. 10   Grain size distribution of V: 5 revolutions at (a) P = 2 GPa and (b) P = 6 GPa.

Fig. 11   Grain size distribution of Mo: 5 revolutions at (a) P = 2 GPa and (b) P = 6 GPa.

Table 1   Grain sizes for V and Mo after HPT process.

Pressure and revolution	V (99.9%)		Mo (99.9%)	
	Center part	Edge part	Center part	Edge part
P = 2 GPa, N = 5	400 nm	380 nm	2870 nm	1580 nm
P = 6 GPa, N = 5	370 nm	330 nm	470 nm	340 nm

overall trend is that the grain size is smaller at the edge part than at the center part, indicating that the grain size is more refined with an increasing amount of strain. Inspection of the SAED patterns indicates also that the misorientation angle of the grain boundary increases with straining because the patterns tend to form a net at the center part and a ring at the edge part. This is consistent with earlier reports that the microstructure evolves from subgrains with low angle boundaries to grains with high angle boundaries with straining by severe plastic deformation. Comparison of the microstructures between V and Mo indicates that the effect of the applied pressure is different: it is little on V so that the microstructure including the grain size formed at 2 GPa is almost the same as the one formed at 6 GPa, but the difference is significant between the two pressures in Mo. It is apparent that subgrain structures well develop not only in the center part but also in the edge part in Mo at the pressure of 2 GPa and the grain size is more than 5 times larger at 2 GPa than at 6 GPa. This microstructural observation is in accordance with the difference in the hardness levels

observed at the two pressures. It is then confirmed that the microstructural evolution is slow in Mo at the applied pressure of 2 GPa. It is considered that this slow evolution of the microstructure is attributed to lower applied pressure with respect to the high yield strength in Mo in contrast with the low yield stress of V. Thus, the generation of dislocation is not sufficient to refine the grain size. It was shown earlier that dislocations play an important role to form grain boundaries with high angle of misorientations.[7] More intense generation of dislocations and less recovery lead to finer grain sizes during severe plastic deformation.[8]

It should be discussed why the microstructure becomes finer in Mo as the applied pressure is higher despite the fact the total strain is the same. It is well established that the strain is determined in proportion to the product of dislocation density and slip distance. Under a high-pressure constrained condition, dislocations are forced to be generated more but at the same time they are forced to be annihilated. This should be less likely when the pressure is low. The saturation level is determined by the balance between dislocation generation and annihilation. The case of larger dislocation density and shorter slip distance at the high-pressure constrained condition yields the same strain as the case of smaller dislocation density and longer slip distance at the low-pressure constrained condition. The difference between the two conditions is that the grain size becomes smaller with higher angle boundaries in the former because the generated dislocations are more annihilated at grain boundaries. The difference

in the microstructure as well as the saturation level arises from the difference in dislocation activity such as generation and annihilation which is more intense at a high-pressure constrained condition than at a low-pressure constrained condition.

6. Summary and Conclusions

(1) Vickers microhardness data of V fall well on a single curve when they are plotted against equivalent strain. The hardness increases with strain and saturates to a constant level. TEM observation reveals that the grain size is reduced to 330~400 nm at the saturation level throughout the sample. The tensile test shows that the strength significantly increases with some ductility reserved. This ductility is consistent with the fractography showing the presence of fine dimples on the fracture surface.

(2) The hardness behavior of Mo is different from V. The hardness values lie on a single curve when the applies pressure is high as 6 GPa but, when it is lower, the hardness increase is gradual to the saturation level, and the hardness level deviates far below the saturation level as the pressure becomes lower. TEM observation reveals that the grain size is reduced to ~350 nm at the saturation level but the microstructure becomes coarser as the applied pressure is lower. The high tensile strength of ~1.4 GPa is achieved at a lower applied pressure as 2 GPa with some ductility but the tensile specimen fractures in a brittle manner when it is processed at the higher pressure of 6 GPa. The difference in the tensile behavior is well reflected in the fractography with fine dimples on the former but with smooth and cleaved surface on the latter.

(3) The slower evolution of microstructure as well as of hardness to the saturation level observed in Mo is due to the applied pressure which is lower than the yield stress so that the dislocation activity is not sufficient to refine the grain size.

Acknowledgements

REFERENCES

1) R. Z. Valiev, R. K. Islamgaliev and I. V. Alexandrov: Prog. Mater. Sci. **45** (2000) 103–189.
2) R. Z. Valiev, Y. Estrin, Z. Horita, T. G. Langdon, M. J. Zehetbauer and Y. T. Zhu: JOM **58** (2006) 33–39.
3) G. Sakai, K. Nkamura, Z. Horita and T. G. Langdon: Mater. Sci. Forum **503–504** (2006) 391–396.
4) N. A. Smirnova, V. I. Levit, V. I. Pilyugin, R. I. Kuznetsov, L. S. Davydova and V. A. Sazonova: Fiz. Met. Metalloved. **68** (1986) 1170–1177.
5) T. Hebesberger, H. P. Stuwe, A. Vorhauer, F. Wetscher and R. Pippan: Acta Mater. **53** (2005) 393–402.
6) A. P. Zhilyaev and T. G. Langdon: Prog. Mater. Sci. **53** (2008) 893–979.
7) K. Edalati, T. Fujioka and Z. Horita: Mater. Sci. Eng. A **497** (2008) 168–173.
8) Y. Ito and Z. Horita: Mater. Sci. Eng. A **503** (2009) 32–36.
9) J. Čížek, I. Procházka, B. Smola, I. Stulíková, R. Kužel, Z. Matěj, V. Cherkaska, R. K. Islamgaliev and O. Kulyasova: Mater. Sci. Eng. A **462** (2007) 121–126.
10) K. Edalati, T. Fujioka and Z. Horita: Mater. Trans. **50** (2009) 44–50.
11) R. Z. Valiev, Yu. V. Ivanisenko, E. F. Rauch and B. Baudelet: Acta Mater. **44** (1996) 4705–4712.
12) Y. Todaka, M. Umemoto, J. Yin, Z. Liu and K. Tsuchiya: Master. Sci. Eng. A **462** (2007) 264–268.
13) F. Wetscher, A. Vorhauer and R. Pippan: Master. Sci. Eng. A **410–411** (2005) 213–216.
14) A. V. Korznikov, S. Idrisova and N. I. Noskova: Phys. Met. Metall. **85** (1998) 327–331.
15) Y. R. Kolobov, B. Kieback, K. V. Ivanov, T. Weissgaerber, N. V. Girsova, Y. I. Pochivalov, G. Grabovetskaya, M. B. Ivanov, V. U. Kazyhanov and I. V. Alexandrov: Int. J. Refract. Met. Hard Mater. **21** (2003) 69–73.
16) R. Wadsack, R. Pippan and B. Schedler: Fusion Eng. Des. **66–68** (2003) 265–269.
17) E. N. Popova, V. V. Popov, E. P. Romanov and V. P. Pilyugin: Phys. Met. Metall. **103** (2007) 407–413.
18) E. N. Popova, V. V. Popov, E. P. Romanov and V. P. Pilyugin: Phys. Met. Metall. **101** (2006) 52–57.
19) Q. Wei, H. T. Zhang, B. E. Schuster, K. T. Ramesh, R. Z. Valiev, L. J. Kecskes, R. J. Dowding, L. Magness and K. Cho: Acta Mater. **54** (2006) 4079–4089.
20) K. Edalati, Z. Horita and T. G. Langdon: Scr. Mater. **60** (2009) 9–12.
21) K. Edalati, E. Matsubara and Z. Horita: Mater. Sci. Eng. A **40** (2009) 2079–2086.
22) K. Edalati, Z. Horita, S. Yagi and E. Matsubara: Mater. Sci. Eng. A **523** (2009) 277–281.
23) K. Edalati, Z. Horita and Y. Mine: Mater. Sci. Eng. A **527** (2010) 2136–2141.